UNIVERSIDAD DISTRITAL
FRANCISCO JOSÉ DE CALDAS

Ingeniería

https://revistas.udistrital.edu.co/index.php/reving/issue/view/1185

DOI: https://doi.org/10.14483/23448393.19845

Research

Characterization of Microbubbles Generated in a Venturi Tube via Image Processing: Effect of Operating Parameters

Caracterización de microburbujas generadas en un tubo Venturi mediante procesamiento de imágenes: efecto de los parámetros operativos

Jhonatan Stiven Mera-Campo[1], Jeimmy Adriana Muñoz-Alegría[2], Juan Fernando Flórez-Marulanda[2]*, and Elena Muñoz-España[2]

[1]Department of Physics, Universidad del Cauca, (Popayán, Colombia)
[2]Department of Electronics, Instrumentation, and Control, Universidad del Cauca, (Popayán, Colombia).

Abstract

Context: This research developed a dissolved air flotation system using a Venturi tube to produce microbubbles. The Venturi tube replaces the saturation tank and the pressure-reducing valve of conventional systems.
Method: The system has both suction and injection air inlets, regulates the recirculation flow of the liquid to the tank, and provides a high hydraulic load in a reduced size. Counting and measuring the microbubbles produced via digital image processing helps to characterize the system's performance.
Results: The system with air suction produces smaller bubbles than that with air injection. A higher liquid recirculation pressure produces more bubbles and reduces their size in the case of air suction.
Conclusions: In air injection, the change in flow rate influences the size of the microbubbles. Air injection and recirculation pressure do not influence the number of bubbles generated.

Keywords: dissolved air flotation, microbubble, Venturi tube, wastewater treatment

Article history

Received:
17th/Aug/2022

Modified:
09th/Nov/2023

Accepted:
04th/Jul/2023

Ing, vol. 28, no. 3, 2023. e19845

*Correspondence: jflorez@unicauca.edu.co

Resumen

Contexto: Esta investigación desarrolló un sistema de flotación por aire disuelto utilizando un tubo Venturi para producir microburbujas. El tubo Venturi sustituye el tanque de saturación y la válvula reductora de presión de los sistemas convencionales.
Método: El sistema tiene entradas de aire tanto por aspiración como por inyección, regula el flujo de recirculación del líquido al tanque y proporciona una alta carga hidráulica en un tamaño reducido. El conteo y la medición por procesamiento digital de imágenes de las microburbujas producidas ayuda a caracterizar el desempeño del sistema.
Resultados: El sistema de succión de aire produce burbujas más pequeñas que el de inyección de aire. Una mayor presión de recirculación del líquido produce más burbujas y reduce su tamaño en el caso de la succión de aire.
Conclusiones: En la inyección de aire, el cambio de caudal influye en el tamaño de las microburbujas. La inyección de aire y la presión de recirculación no influyen en el número de burbujas generadas.

Palabras clave: flotación por aire disuelto, microburbujas, tubo Venturi, tratamiento de aguas residuales

Table of contents

1. Introduction

Environmental regulations stimulate research on wastewater purification and treatment (1). Conventional treatment methods involve microbial metabolism (2); the coagulation of colloid particles and solids in the water, selecting the coagulant according to the wastewater; membrane separation, trapping contaminant particles; and flotation or addition of gas bubbles, where the particles suspended in the water rise to the surface attached to the bubbles (3). Treatment methods have a contaminant removal efficiency that depends on the design, the size of the equipment, and the materials used.

In flotation methods, the particle-bubble collision probability influences the removal efficiency. The bubble must be smaller than the contaminant's particle size (4). Several flotation techniques include

a cyclonic static microbubble flotation column (5, 6). The combination of flotation columns, cyclone separation, and microbubble generators yields bubbles of less than 10 μm in diameter and has a removal efficiency of 92,19 %. Electro-flotation (7) separates solid particles with bubbles between 15 and 80 μm in diameter which are produced by electrodes. Its separation efficiency is 64,5 %. In dissolved air flotation (DAF) (8), water saturated with pressurized air is passed through a pressure-reducing valve to generate microbubbles of 20-100 μm. This method has a removal efficiency of 90 %. At the industrial level, one of the main contaminants is grease. Industrial grease removal uses the DAF and induced air flotation (IAF) methods (9). The IAF method requires a more extensive setup than DAF. For an effective removal of contaminants and an adequate size reduction, the DAF method offers high efficiency by removing suspended grease particles while having a less complex setup in comparison with other flotation techniques (10).

The DAF method produces bubbles with characteristics such as larger gas-liquid surface area, higher gas retention, and slower rising velocity in order to achieve a high contaminant removal (11). The bubble size distribution influences these properties (12). Macro-bubbles have a high rising velocity and low collision with contaminant particles. Microbubbles decrease in size as they rise until they burst due to stagnation. Nanobubbles remain suspended in the water for longer periods of time without bursting (11). The DAF method uses microbubbles to increase the contaminant removal efficiency and flow velocity (13). The characteristics of microbubbles for flotation treatment are diameters ranging from 1 to 200 μm and an increased bubble inertial pressure with decreasing diameter without collapsing. The area-volume ratio is inversely proportional to the diameter. Cavitation pertains to the formation, growth, and collapse of bubbles (14). Hydrodynamic cavitation produces bubbles by pressure variation with increasing liquid velocities, and it is a low-cost, energy-efficient method (15). Other types of cavitation are acoustic fields, laser light photons, and elementary particles (16). The type of cavitation influences the bubble production efficiency, the equipment footprint, and the associated costs.

Some hydrodynamic cavitation methods involve a spherical body in a tube through which a liquid flows, generating bubbles by the decay of the internal pressure at the constriction of the channel (17). Others utilize the spiral injection of a fluid with a pump in a specific flow zone, reducing the pressure in its central axial part, generating bubbles by gas suction (18). In others, the fluid passes through a Venturi tube, which increases its velocity and reduces its pressure. The gas is self-primed from the low-pressure point and remains mixed with the liquid (19). Furthermore, pressurized solution injection involves injecting an air-water mixture at a pressure of 3-4 atm into a tank at atmospheric pressure. The pressure change causes the supersaturated air to form microbubbles in the water (4). Pressurized dilution is commonly used within the framework of the DAF method. Studies on microbubble generation via Venturi tubes range from laboratory to industrial scales, with bubbles suitable for grease removal in water (12, 19).

The shape, size, motion, forces, and surrounding physicochemical environment make microbubble characterization difficult (20). There are several techniques to determine microbubble parameters, ranging from intrusive to non-intrusive methods (21). In recent years, high-speed camera photography has been used for microbubble characterization. This non-intrusive method is easy to use in industrial

environments and is less expensive than electronic equipment (22,23) Calibration for image acquisition affects the accuracy of image processing. Camera calibration methods analyze real objects with known measurements. The intrinsic and extrinsic parameters of a camera are extracted from a set of correspondences between real three-dimensional points and two-dimensional image points (24). The calibration of electronic devices is more complex than that of cameras (25,26). In fact, the potential use of smartphone cameras for microbubble measurement has not yet been investigated.

This research implemented a DAF system with a Venturi tube microbubble generation method, analyzing the influence of the liquid recirculation pressure, the inlet type, and the airflow rate on microbubble production. The characterization of the diameter and the count of microbubbles generated was performed via a measurement system based on digital image processing installed in the contact zone of the DAF tank. This low-cost microbubble measurement system uses a smartphone camera to measure the diameter and count the microbubbles generated in a lab-scale DAF system at room temperature with clean water. The microbubble measurement algorithm developed in MATLAB (under a campus-wide license) allows for a fast and detailed characterization of dense bubble populations with different diameters.

2. Materials and methods

2.1. Venturi tube design and construction

According to Bernoulli's equation, when a liquid flows through a pipe, its velocity increases and its pressure decreases as the cross-sectional area of the pipe narrows. The air suction created in the narrowed or low-pressure area of a Venturi tube aids in the formation of bubbles. Air can be introduced into the tube by drawing it from the atmosphere or by injection using a pneumatic compressor. To produce microbubbles in the desired area, the geometric parameters of the tube must be considered, *i.e.*, the throat diameter, inlet angle, cone diameter, suction diameter, cone length, and outlet angle (Fig. 1). The parameters with the greatest influence on microbubble size are the inlet and outlet angles of the Venturi tube (27).

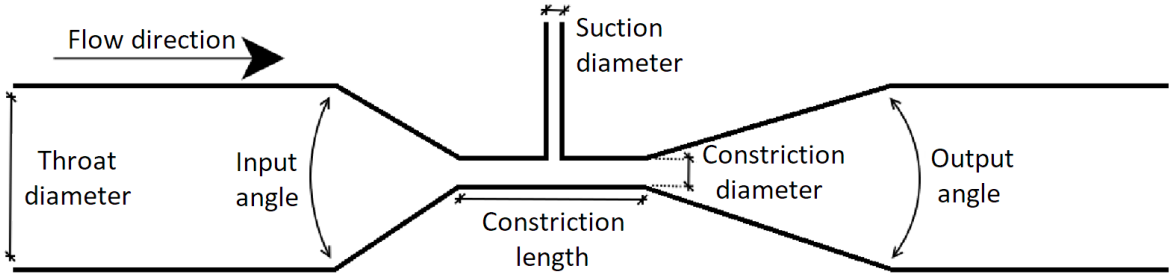

Figure 1. Geometric parameters of a Venturi tube

As the liquid flow increases at the inlet of a Venturi tube, the bubble size decreases if the inlet angle is large relative to the outlet angle. The progressive increase in the orifice diameter to a value smaller than the throat diameter causes a gradual increase in pressure and a decrease in liquid velocity, thus increasing the cavitation intensity. To optimize the size of the generated microbubble, it is necessary for the inlet angle and throat diameter to be at least twice as large as the outlet angle and the narrowing diameter, respectively (27). According to the influence of the geometrical parameters (Fig. 1), the authors of (28) provide some considerations regarding their optimal values. These parameters (Table I) allowed elaborating a CAD design (Fig. 2a) for 3D-printing in PLA (Fig. 2b).

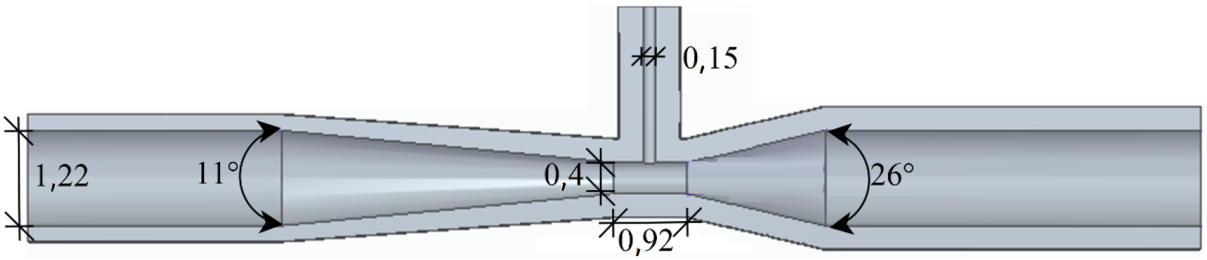

a. CAD design of the tube (dimensions in cm)

b. Printed tube

Figure 2. Developed Venturi tube

Table I. Venturi tube design parameters

Parameter	Measure	Parameter	Measure
Liquid inlet angle	26°	Narrowing length	0,92 cm
Liquid outlet angle	11°	Suction diameter	0,15 cm
Throat diameter	1,22 cm	Tube thickness	0,3 cm
Narrowing diameter	0,4 cm		

2.2. DAF tank design and construction

In the developed DAF system, the recirculation of the liquid through the Venturi tube produces pressurization and mixing with air (29). According to the operation and resistance of the developed Venturi tube (Fig. 2), the maximum recirculation flow rate is 16 L/min. In order to achieve a high rate of rising suspended particles, the design of the proposed flotation tank follows previous models (30), with internal structures for higher efficiency, lower cost, and smaller size (Fig. 3).

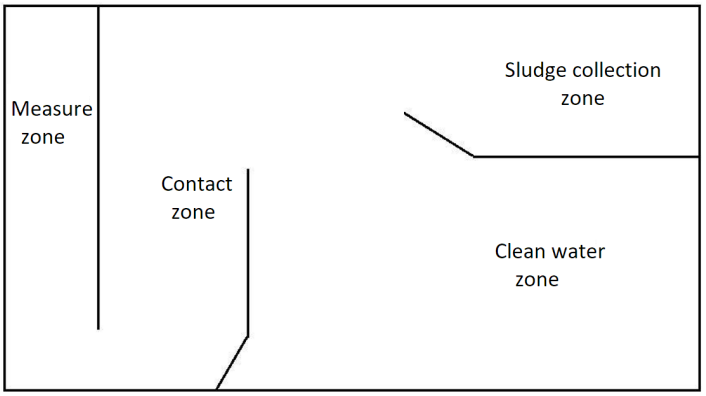

a. Zone distribution

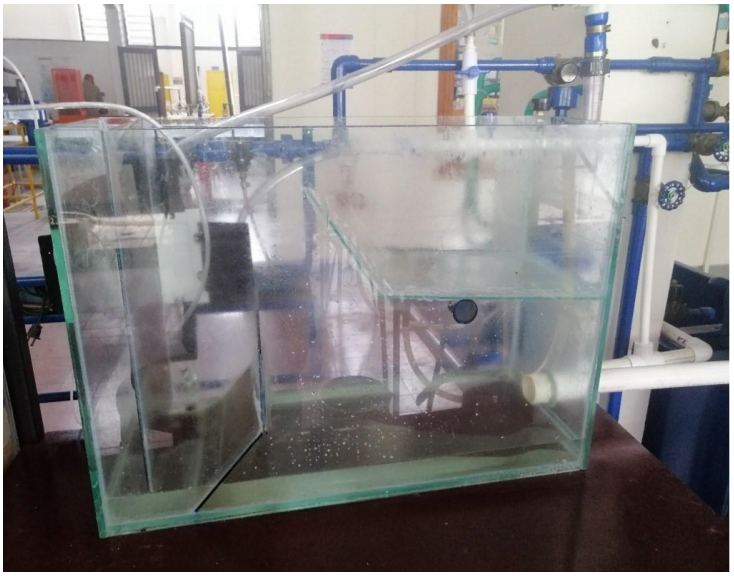

b. Constructed assembly

Figure 3. Developed flotation tank

The four internal zones of the flotation tank are:

- The *measurement zone*, a space in which a portion of the bubbles is periodically lifted, facilitates the acquisition of microbubble images for measurement.
- The *contact zone* is an area of higher concentration of microbubbles and contact with grease

particles in the liquid to be treated.

- In the *clean liquid zone*, the treated liquid flows to another tank and recirculates.
- The *sludge collection area* is a tank for collecting the removed grease particles.

Prior to construction, the CAD design of the flotation tank provides external and internal measurements (Fig. 4). The 53° deflector angle (Fig. 4b) produces a high hydraulic load on the flotation tank, together with a size reduction, without causing turbulence in the contaminants, thus avoiding the re-mixing of contaminants with the treated liquid.

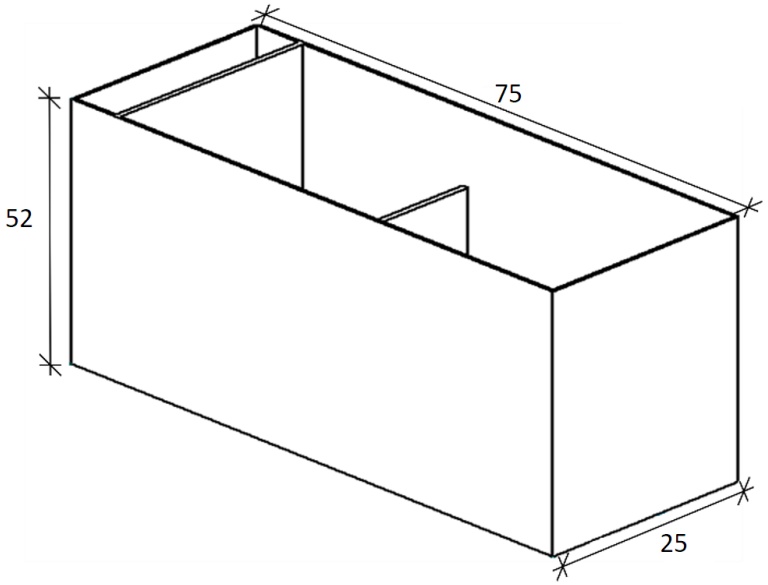

a. External dimensions

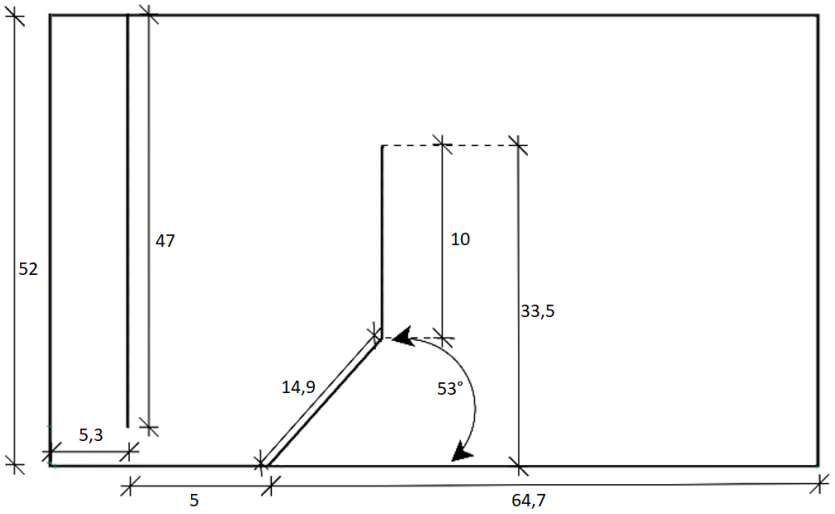

b. Internal dimensions

Figure 4. CAD design of the flotation tank (measurements in cm)

The design parameters of DAF systems are as follows.

- The ratio of kilograms of air used to kilograms of solids separated for high concentrations of solids in the effluent is expressed by Eq. (1) (31):

$$\frac{A_a}{S} = \frac{1,3S_a(fP-1)}{S_s} \tag{1}$$

Where:
A_a/S: air-solids ratio, ml/mg
A_a: Air requirement kg/h
S_a: solubility in air ml/l
F: Fraction of dissolved air at a pressure P
P: Pressure atm
S_s: Influent suspended solids, g/m^3 (mg/L)

- The hydraulic loading (HL) is the total flow rate per unit area (Q/A) (32). The total flow is shown in Eq. (2):

$$Q = Q_{AR} + Q_R \tag{2}$$

where Q_{AR} is the treatment flow rate and Q_R is the recirculation flow rate, expressed as Eq. (3):

$$Q_R = \frac{A_a}{\alpha X_S^P} \tag{3}$$

Here, X_S^P is the solubility of air in pure water at the working temperature and pressure (for temperatures between 20 and 30 °C, it varies between 18 and 15 ppm), and α is the impurity coefficient of the wastewater (nominal values are between 0,60 and 0,80) (33).

- The recirculation rate (%R) is the ratio of the recirculation flow and the total flow.
- The hydraulic retention time (HRT), which indicates the residence time of the water to be treated in the flotation tank, is the ratio between the volume of water to be treated (V) and the total flow rate.

The design of the flotation tank and the Venturi tube determine the parameter values of the developed DAF system (Table **II**). The efficiency varies according to the ratio between the kilograms of air used and the kilograms of separated solids (A/S), with values between 0,005 and 0,09 (30).

2.3. DAF system instrumentation

The developed system includes a flotation tank for removing contaminant particles; a tank for water treatment, with liquid temperature control and a mechanical stirrer for mixing and temperature homogenization; an auxiliary tank to receive the treated water; two 2 HP motor pumps with a flow rate of 20 L/min, the first of which is responsible for the water flowing through the hydraulic circuit and the second for the removal of the separated sludge from the collection area of the flotation tank; three 1 inch light gate valves and four 1/2 inch unthreaded PVC ball valves; and a portable pneumatic compressor for injecting air into the Venturi tube.

Table II. Flotation tank design parameters

Parameter	units	Calculated value
HL	m/h	5,12
HRT	min	3,25
%R	%	0,53
Q_R	m^3/min	0,016
QAR	m^3/min	0,014
Q	m^3/min	0,03
A_a	kg/h	0,008568

The DAF system's flotation tank uses 1 cm thick glass, and the partitions inside it use 4 mm thick glass. The holding and auxiliary tanks are made of plastic and have a capacity of 160 L. The system uses a water rotameter (0-1.000 L/h) and a pressure gauge (0-60 psi) to measure the flow rate and the recirculation pressure from motor pump 1 to the Venturi tube. To measure the airflow into the Venturi tube, an air rotameter is used (0,3-0,5 L/min) (Fig. 5).

Figure 5. Developed DAF system

The Venturi tube is located at 3 cm from the bottom of the flotation tank. The coupling of the Venturi tube and the hydraulic circuit uses a 3/4 inch, 2 mm thick transparent hose. The air inlet uses a 1/8 inch, 1 mm thick hose for the duct leading to the narrowing zone (Fig. 6).

2.4. Microbubble measurement system

The main components of the microbubble measurement system are a 20-megapixel Huawei Mate 20 Lite smartphone camera with a 3X digital zoom, F/1,8 aperture, a 5.120 x 3.840 pixel resolution per

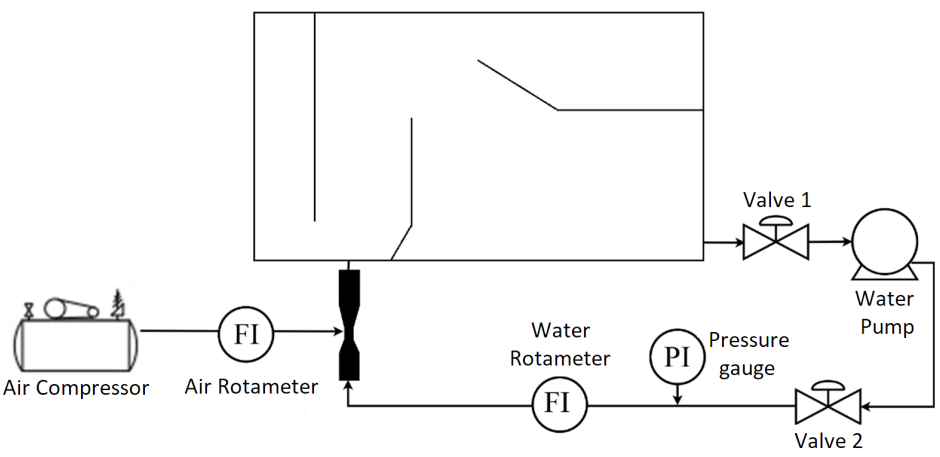

Figure 6. Flow diagram of the microbubble generation process

frame, and slow-motion recording features. The smartphone camera has a 15X macro lens, and images are captured in an area of 1,8 x 2,2 cm with an 18 W LED lamp lighting system at 110 Vac located backlit to the camera. The experimental setup components and adjustment accessories cost approximately 300 USD (Fig. 7).

A code developed offline in MATLAB measures the diameters and microbubble counts of the captured

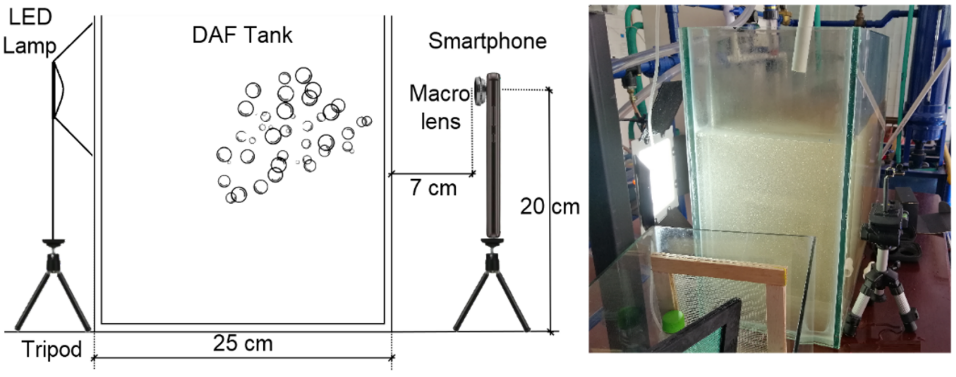

Figure 7. Microbubble measurement system developed

images, all of which are taken while the DAF system runs on clean water. The microbubble images are extracted from a 1.280 x 720-pixel slow-motion video featuring 20 seconds of operation as recorded by the measurement system. There is a two-second interval between each frame analyzed, resulting in a total of 10 images. Image processing is performed in three steps:

1. *Thresholding by V-plane*: In this case, a value of 0,95 is determined by trial and error, obtaining more detail than automatic thresholding segmentation methods.
2. *Application of MATLAB correction filters (imdilate, imfill, imclearborder):* In each thresholded image, two white fringes are generated by the surfaces bounding the measurement area. The filters remove these fringes and fill the gaps inside the microbubble borders.

3. *Microbubble measurement using the imfindcircles MATLAB function:* For each 1. 280 x 720-pixel image, this function calculates the number and pixel radii of the microbubbles. With the radius of each bubble, the average and the standard deviation are calculated. Finally, the pixel size ratio converts these pixel values to μm. In this case, each pixel is 5,79 μm.

The microbubble measurement algorithm was developed in MATLAB 2019a and executed on a desktop computer with an Intel i3 processor, 8 GB RAM, an MSI Gt 730 4 GB Oc graphics card, and a Windows 10 operating system with a 64-bit architecture. The measurement algorithm takes 3 to 4 min to process the images (Fig. 8).

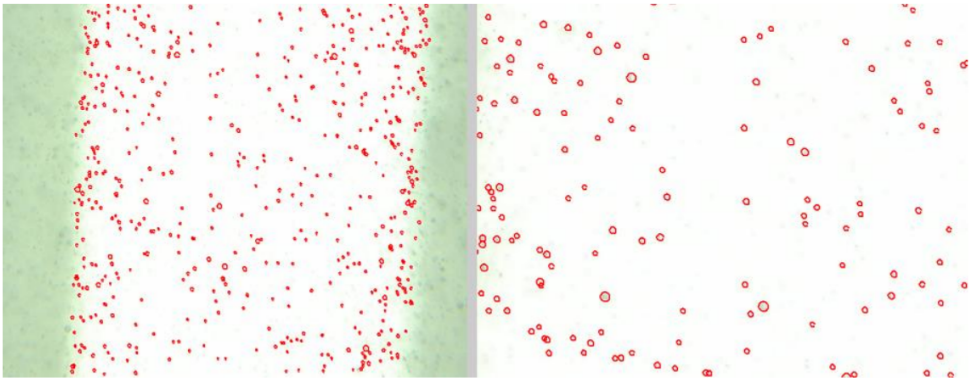

Figure 8. Circle detection: standard image on the left, zoomed region of the image on the right

3. Results and discussion

The microbubble production of the proposed system helps to analyze the influence of recirculation pressure and the inlet air flow rate to the Venturi tube on the size of microbubbles created by air suction and injection.

3.1. Hydrodynamic cavitation with air suction

The DAF system works with an air suction of less than 0,3 L/min, as higher values produce macrobubbles. In this case, there is a variation in pressure and recirculation flow (Fig. 9), which determines the number and diameter of the microbubbles produced. At an initial recirculation flow rate of 16 L/min, the pressure is 36 psi. Reducing the flow rate through the recirculation line produces a pressure of 34 psi.

The increase in recirculation pressure from 34 to 36 psi reduces the diameter of the bubbles. The average diameter for the two pressures differs by 4 μm. At 36 psi, a bubble diameter of 134,90 μm corresponds to 52 % of the bubbles generated. At 34 psi, this percentage drops to 32 % for the same diameter. 34 % of the bubbles generated at 34 psi have a diameter of 161,00 μm. At both pressures, bubble diameter values between 134,90 and 161,00 μm are generated: 82 % of the population at 36 psi and 66 % at 34 psi. The average number of bubbles detected per area is 1.143 at 36 psi and 531 at 34 psi.

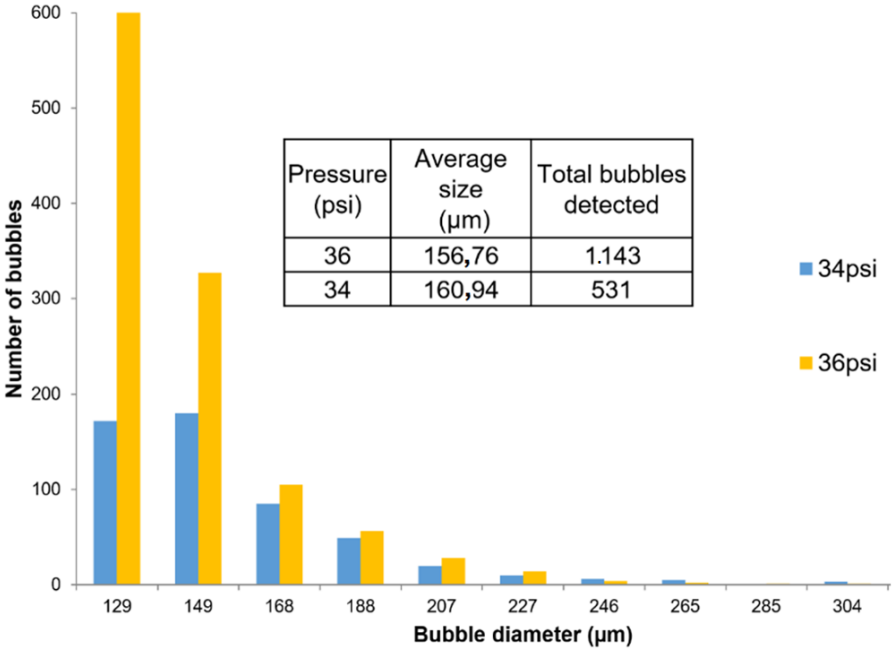

Figure 9. Microbubble population at recirculation pressures of 36 and 34 psi

3.2. Hydrodynamic cavitation with air injection

A 2^2 factorial design (Table III) was used to analyze the average diameter and number of bubbles produced by air injection. Its evaluation factors are the air injection flow rate (0,3 and 0,5 L/min) and the recirculation pressure (36 and 34 psi). There are four measurements for each combination.

Table III. Evaluation combinations regarding air injection

Air injection	Repetition	34 psi				36 psi			
		D (μm)	σD	N	σN	D (μm)	σD	N	σN
0,3 L/min	1	160,5588	18,4615	251	24,03	160,7424	18,4761	258	13,63
	2	160,6102	18,5416	218	28,69	160,7314	18,4779	243	15,73
	3	160,4565	18,4620	254	26,72	160,7364	18,4147	271	15,31
	4	160,3694	18,4615	252	24,03	160,7421	18,4759	260	13,45
0,5 L/min	1	161,3271	18,7146	242	13,4	161,0551	19,3956	260	16,15
	2	161,8995	18,7151	223	16,72	161,7751	19,3495	237	18,31
	3	161,3271	18,7136	242	13,4	161,0552	19,7285	236	18,41
	4	161,2013	18,7146	244	13,65	161,0551	19,3945	264	16,32

The results of the factorial design (α-value of 0,05, Table IV), indicate, with a p-value of 0,886, that the average bubble diameter does not vary significantly for different recirculation pressures. The p-value of $7,49 \times 10^{-5}$ indicates that the variation in the air injection flow rate affects the size of the microbubbles. On the other hand, the air flow rate, with a p-value of 0,3014, and the recirculation pressure (0,0838)

have no influence on the number of bubbles generated. In no case does the variation of the parameters in combination influence the size and number of microbubbles.

Table IV. Results of the factorial design for air injection

	Microbubble size				
	Sum Sq.	**Mean Sq.**	**F-value**	**P-value**	**Confidence intervals, percentile 95 %**
	Microbubble size				
Pressures	0,0013	0,0013	0,021	0,886	[-0,248; 0,284]
Flow rates	2,0652	2,0652	34,564	7,49e-05	[0,452; 0,984]
Pressure-Flow	0,1962	0,1962	3,284	0,095	[-0,717; 1,453]
	Microbubble density				
Pressures	663,1	663,2	3,555	0,0838	[-2,003; 27,753]
Flow rates	217,6	217,7	1,166	0,3014	[-22,253; 7,503]
Pressure-flow	7,6	7,6	0,041	0,8438	[-48,921; 42,921]

3.3. Oil and grease removal

The cleaning tests consist of treating the synthetic domestic wastewater with the DAF prototype for 16 min. During the first minute, the system stabilizes at the set recirculation pressure and air injection. In the next seven minutes, the system forms a small region of foam or suspended solids. Within the next eight minutes, the system has a visible layer of solids, particularly the presence of oils and grease, which, in this case, were analyzed at Corporación Autónoma Regional del Cauca's laboratory using the SM5520D Soxhlet method.

For each pair of parameters (34 psi at a 0,1 L/min air injection and 36 psi at a 0,1 L/min air injection), five cleaning tests were performed, with a new Venturi tube for each one, measuring the oil and grease concentration (Table V). The average grease and oil removal at 34 psi was 89,22 %, as well as 83,64 % at 36 psi. An ANOVA test, with an α-value of 0,05 and a p-value of 0,038, indicates a difference between the two evaluated parameter levels.

3.4. Discussion

By comparing both models for microbubble generation according to the smaller diameters obtained, it can be stated that air injection produces bubbles of a larger average size (160 μm) than air suction (156 μm). A higher air flow rate increases the amount of dissolved air in the water, which requires an increased recirculation pressure to break up the air cloud. Likewise, the increased air reduces the number of bubbles generated by the low air breakup. The bubbles are larger because of the larger amount of air, preventing the generation of new bubbles.

Table V. Oil and grease removal efficiencies

Concentration of untreated oils and grease	Recirculation pressure: 34 psi; air injection: 0,1 L/min		Recirculation pressure: 36 psi; air injection: 0,1 L/min	
	Oil and grease concentration DAF treatment		Oil and grease concentration DAF treatment	
(mg/L)	(mg/L)	Efficiency (%)	(mg/L)	Efficiency (%)
589	95,3	83,82	103	82,51
589	75,6	87,16	99,5	83,11
589	23,8	95,96	107	81,83
589	67,1	88,61	73,6	87,50
589	55,8	90,53	98,6	83,26

For most of the characteristics evaluated, there is no significant difference in the variation of the recirculation pressure. However, at a practical level, according to the results obtained, it is advisable to work with 34 psi, as it generates a lower cavitation effect in the Venturi tube and a lower power consumption of the system and the tests performed with synthetic domestic wastewater. This pressure reported a higher percentage of grease and oil removal.

The results show that the Venturi tube produces bubbles suitable for DAF systems. The Venturi tube replaces the saturation tank and the pressure-reducing valve in the proposed system. These components account for 10 to 30 % of the total costs in conventional DAF systems (27). Implementing our proposal on an industrial scale would result in a minimum 10 % reduction in the cost of conventional DAF systems, as well as a reduction in the space required for installation.

The advent of modern cameras and computer processing power allows for the automatic online and offline monitoring of bubbles (21), as shown in Table **VI**. Nevertheless, it is necessary to calibrate the camera with a high accuracy, as this affects the performance and estimation of extrinsic and intrinsic parameters (24, 34, 35). The use of digital image processing equipment with offline or online algorithms costs more than 1.000 USD. The developed system generates an offline MB measurement with low computational cost and fast response times, which allows to take different samples in the field and make control decisions directly.

Regarding the location of the camera to measure microbubbles in DAF systems, measurement is typically performed at the top of the tank (40, 41). At this point, the bubbles have reached their maximum size, and their removal capacity is reduced. Another way is to take a sample of the generated bubbles (38, 43). In this case, the bubbles are measured before they reach their maximum size. However, changes in the uncontrolled environment of the bubbles may cause the analyzed sample to be unrepresentative. The developed microbubble measurement system performs a direct measurement of the bubbles generated by placing the chamber in the contact zone of the DAF tank, providing an adequate characterization of the generated microbubbles in order to determine their possible use in the removal of contaminants. Regardless of the location of the camera, any microbubble measurement

Table VI. Offline and online methods for microbubble measurement

Techniques	Offline Online	Bubble parameter	Processing time (s)	Ref.
First version algorithm	Offline	BSD-velocity-trajectory	-	(36)
Concave point extraction algorithm	Offline	BSD-diameter	-	(37)
CHT-Single bubble Algorithm	Online	BSD-diameter	60-300	(38)
CHT-CNN-CCA-WaldBoost+LBP-Trees CNN	Online	BSD-diameter	-	(39)
WaldBoost+Trees	Online	Bubble detection	120-180	(40)
Watershed algorithm	Offline	Bubble detection	-	(41)
Watershed algorithm-CHT	Online	BSD-diameter	-	(42)
DFT-Otsu algorithm	Online	BSD-diameter	0,03-0,18	(43)
GSC	Online	Bubble detection	120	(44)
CCA	Online	Bubble detection	40	(45)

system with digital image processing must have adequate lighting and adjust the chamber exposure parameters according to the characteristics of the environment in which the DAF system is located.

4. Conclusions

This research developed a DAF system using a Venturi tube microbubble generation method. The system replaces the saturation tank and the pressure-reducing valve of conventional systems, which leads to a reduction in the size of the proposed DAF system without affecting the hydraulic load. A microbubble measurement system counts and measures the microbubbles.

The proposed DAF system allows varying the recirculation pressure of the treated water and an air inlet by air injection or suction. The analysis of the variations in recirculation pressure and the inlet air flow rate evidenced the influence of these parameters on the quantity and size of the microbubbles generated. Regarding the combinations of parameters analyzed, the DAF system with a suction inlet air flow rate of less than 0,3 L/min and a treated water recirculation pressure of 36 psi generates a high number of microbubbles with the smallest possible size. In the case of air injection, increasing the inlet air flow rate generates an increase in microbubble size. There is no influence on the number of bubbles generated for any given air flow rate and recirculation pressure.

Digital image processing is convenient for the estimation of microbubble parameters. The developed microbubble measurement system costs about 300 USD, a value below the equipment that is often used in research. For adequate detection and measurement, it is necessary to obtain images with a distinction between the background and the air bubbles, generating a good definition of the perimeter. The images in this study were taken with an ISO value of 320 and a shutter speed of 1/1.000 in an area of 1,8 x 2,2 cm.

5. CRediT author statement

Jhonnatan Stiven Mera Campo: Methodology, investigation, software, writing – original draft.
Jeimmy Adriana Muñoz Alegria: Methodology, investigation, software, writing – original draft.
Juan Fernando Flórez Marulanda: Conceptualization, formal analysis, validation, and writing – original draft.
Elena Muñoz España: Data visualization, investigation, supervision, and writing – review.

References

[1] C. Li, J. Li, N. Wang, Q. Zhao, and P. Wang, "Status of the treatment of produced water containing polymer in oilfields: A review," *J. Environ. Chem. Eng.*, vol. 9, no. 4, art. 105303, 2021. https://doi.org/10.1016/j.jece.2021.105303 ↑2

[2] L. Yu, M. Han, and F. He, "A review of treating oily wastewater," *Arabian J. Chem.*, vol. 10, pp. S1913-S1922, 2017. https://doi.org/10.1016/j.arabjc.2013.07.020 ↑2

[3] G. L. Muniz, A. C. Borges, and T. C. F. da Silva, "Performance of natural coagulants obtained from agro-industrial wastes in dairy wastewater treatment using dissolved air flotation," *J. Water Process Eng.*, vol. 37, art. 101453, 2020. https://doi.org/10.1016/j.jwpe.2020.101453 ↑2

[4] R. Prakash, S. K. Majumder, and A. Singh, "Flotation technique: Its mechanisms and design parameters," *Chem. Eng. Processing-Process Intens.*, vol. 127, pp. 249-270, 2018. https://doi.org/10.1016/j.cep.2018.03.029 ↑2, 3

[5] G. Pooja, P. S. Kumar, and S. Indraganti, "Recent advancements in the removal/recovery of toxic metals from aquatic system using flotation techniques," *Chemosphere*, vol. 287, art. 132231, 2022. https://doi.org/10.1016/j.chemosphere.2021.132231 ↑3

[6] X. Yan, S. Meng, A. Wang, L. Wang, and Y. Cao, "Hydrodynamics and separation regimes in a cyclonic-static microbubble flotation column," *Asia-Pacific J. Chem. Eng.*, vol. 13, no. 3, art. e2185, 2018. https://doi.org/10.1002/apj.2185 ↑3

[7] R. Mohtashami and J. Q. Shang, "Electroflotation for treatment of industrial wastewaters: a focused review," *Env. Proc.*, vol. 6, no. 2, pp. 325-353, 2019. https://doi.org/10.1007/s40710-019-00348-z ↑3

[8] F. C. P. e Silva, N. M. P. e Silva, J. M. Luna, R. D. Rufino, V. A. Santos, and L. A. Sarubbo, "Dissolved air flotation combined to biosurfactants: a clean and efficient alternative to treat industrial oily water," *Rev. Environ. Sci. Biotechnol.*, vol. 17, no. 4, pp. 591-602, 2018. https://doi.org/10.1007/s11157-018-9477-y ↑3

[9] Z. Khan *et al.*, "Current developments in esterification reaction: A review on process and parameters," *J. Ind. Eng. Chem.*, vol. 103, pp. 80-101, 2021. https://doi.org/10.1016/j.jiec.2021.07.018 ↑3

[10] D. Mesa and P. R. Brito-Parada, "Scale-up in froth flotation: A state-of-the-art review," Sep. *Purif. Technol.*, vol. 210, pp. 950-962, 2019. https://doi.org/10.1016/j.seppur.2018.08.076 ↑3

[11] M. Alheshibri, J. Qian, M. Jehannin, and V. S. J. Craig, "A history of nanobubbles," *Langmuir*, vol. 32, no. 43, pp. 11086-11100, 2016. https://doi.org/10.1021/acs.langmuir.6b02489 ↑3

[12] A. Gordiychuk, M. Svanera, S. Benini, and P. Poesio, "Size distribution and Sauter mean diameter of micro bubbles for a Venturi type bubble generator," *Exp. Therm. Fluid. Sci.*, vol. 70, pp. 51-60, 2016. https://doi.org/10.1016/j.expthermflusci.2015.08.014 ↑3

[13] K. H. A. L. Mahmood, S. J. Wilkinson, and W. B. Zimmerman, "Airlift bioreactor for biological applications with microbubble mediated transport processes," *Chem. Eng. Sci.*, vol. 137, pp. 243-253, 2015. https://doi.org/10.1016/j.ces.2015.06.032 ↑3

[14] T. Temesgen, T. T. Bui, M. Han, T. Kim, and H. Park, "Micro and nanobubble technologies as a new horizon for water-treatment techniques: A review," *Adv. Colloid Interface Sci.*, vol. 246, pp. 40-51, 2017. https://doi.org/10.1016/j.cis.2017.06.011 ↑3

[15] N. Asaithambi, P. Singha, M. Dwivedi, and S. K. Singh, "Hydrodynamic cavitation and its application in food and beverage industry: A review," *J. Food Process Eng.*, vol. 42, no. 5, art. e13144, 2019. https://doi.org/10.1111/jfpe.13144 ↑3

[16] N. Nirmalkar, A. W. Pacek, and M. Barigou, "On the existence and stability of bulk nanobubbles," *Langmuir*, vol. 34, no. 37, pp. 10964-10973, 2018. https://doi.org/10.1021/acs.langmuir.8b01163 ↑3

[17] Y. Yoo *et al.*, "Method for Determining Optimum Operational Conditions of Microbubble Scrubber Using Image Processing.," *J. Environ. Informatics*, vol. 38, no. 2, pp. 83-92, 2021. https://doi.org/10.3808/jei.202100457 ↑3

[18] I. v Naumov, B. R. Sharifullin, and V. N. Shtern, "Vortex breakdown in the lower fluid of two-fluid swirling flow," *Phys. Fluids*, vol. 32, no. 1, art. 14101, 2020. https://doi.org/10.1063/1.5132584 ↑3

[19] C. H. Lee, H. Choi, D.-W. Jerng, D. E. Kim, S. Wongwises, and H. S. Ahn, "Experimental investigation of microbubble generation in the venturi nozzle," *Int. J. Heat Mass Transf.*, vol. 136, pp. 1127-1138, 2019. https://doi.org/10.1016/j.ijheatmasstransfer.2019.03.040 ↑3

[20] B. Swart *et al.*, "In situ characterisation of size distribution and rise velocity of microbubbles by high-speed photography," *Chem. Eng. Sci.*, vol. 225, art. 115836, 2020. https://doi.org/10.1016/j.ces.2020.115836 ↑3

[21] F. Noelle, M. R. Molteno, and R. W. M. Pott, "Calibrated bubble depth determination using a single camera," *Chem. Eng. Res. Design*, vol. 164, pp. 11-22, 2020. https://doi.org/10.1016/j.cherd.2020.09.023 ↑3, 14

[22] M. Lichti and H.-J. Bart, "Bubble size distributions with a shadowgraphic optical probe," *Flow Meas. Inst.*, vol. 60, pp. 164-170, 2018. https://doi.org/10.1016/j.flowmeasinst.2018.02.020 ↑4

[23] R. Prakash, S. Kumar Majumder, and A. Singh, "Bubble size distribution and specific bubble interfacial area in two-phase microstructured dense bubbling bed," *Chem. Eng. Res. Design*, vol. 156, pp. 108-130, 2020. https://doi.org/10.1016/j.cherd.2020.01.032 ↑4

[24] X. Chen *et al.*, "Fourier-transform-based two-stage camera calibration method with simple periodical pattern," *Opt. Lasers Eng.*, vol. 133, art. 106121, 2020. https://doi.org/10.1016/j.optlaseng.2020.106121 ↑4, 14

[25] P. F. Fazzini, P. G. Merli, and G. Pozzi, "Electron microscope calibration for the Lorentz mode," *Ultramicroscopy*, vol. 99, no. 2, pp. 201-209, 2004. https://doi.org/10.1016/j.ultramic.2004.01.002 ↑4

[26] Q. Zhang, H. Xie, W. Shi, and B. Fan, "A novel sampling moiré method and its application for distortion calibration in scanning electron microscope," *Opt. Lasers Eng.*, vol. 127, art. 105990, 2020. https://doi.org/10.1016/j.optlaseng.2019.105990 ↑4

[27] M. Li, A. Bussonnière, M. Bronson, Z. Xu, and Q. Liu, "Study of Venturi tube geometry on the hydrodynamic cavitation for the generation of microbubbles," *Miner. Eng.*, vol. 132, pp. 268-274, 2019. https://doi.org/10.1016/j.mineng.2018.11.001 ↑4, 5, 14

[28] Y. Xiong and F. Peng, "Optimization of cavitation venturi tube design for pico and nano bubbles generation," *Int. J. Min. Sci. Technol.*, vol. 25, no. 4, pp. 523-529, 2015. https://doi.org/10.1016/j.ijmst.2015.05.002 ↑5

[29] P. Mavros and K. A. Matis, *Innovations in Flotation Technology*, Dodrecht, Netherlands: Springer Science & Business Media, 2013. ↑6

[30] P. Palaniandy, M. N. Adlan, H. A. Aziz, M. F. Murshed, and Y.-T. Hung, "Dissolved air flotation (DAF) for wastewater treatment," *Waste Treat. Serv. Utility Ind.*, pp. 145-182, 2017. https://doi.org/10.1201/b22213-5 ↑6, 8

[31] M. Salgot and M. Folch, "Wastewater treatment and water reuse," *Curr. Opin. Environ. Sci. Health*, vol. 2, pp. 64-74, 2018. https://doi.org/10.1016/j.coesh.2018.03.005 ↑8

[32] P. Pazouki, R. A. Stewart, E. Bertone, F. Helfer, and N. Ghaffour, "Life cycle cost of dilution desalination in off-grid locations: A study of water reuse integrated with seawater desalination technology," *Desalination*, vol. 491, art. 114584, 2020. https://doi.org/10.1016/j.desal.2020.114584 ↑8

[33] M. A. Santos, F. Capponi, C. H. Ataíde, and M. A. S. Barrozo, "Wastewater treatment using DAF for process water reuse in apatite flotation," *J. Clean. Prod.*, vol. 308, art. 127285, 2021. https://doi.org/10.1016/j.jclepro.2021.127285 ↑8

[34] X. Lin, J. Song, X. Chen, and H. Yang, "Ultrasound-activated sensitizers and applications," *Angewandte Chemie Int. Ed.*, vol. 59, no. 34, pp. 14212-14233, 2020. https://doi.org/10.1002/anie.201906823 ↑14

[35] H. He, H. Li, Y. Huang, J. Huang, and P. Li, "A novel efficient camera calibration approach based on K-SVD sparse dictionary learning," *Measurement*, vol. 159, art. 107798, 2020. https://doi.org/10.1016/j.measurement.2020.107798 ↑14

[36] M. Qadafi, S. Notodarmojo, and Y. Zevi, "Effects of microbubble pre-ozonation time and pH on trihalomethanes and haloacetic acids formation in pilot-scale tropical peat water treatments for drinking water purposes," *Sci. Total Env.*, vol. 747, art. 141540, 2020. https://doi.org/10.1016/j.scitotenv.2020.141540 ↑15

[37] S. Zhong, X. Zou, Z. Zhang, and H. Tian, "A flexible image analysis method for measuring bubble parameters," *Chem. Eng. Sci.*, vol. 141, pp. 143-153, 2016. https://doi.org/10.1016/j.ces.2015.10.033 ↑15

[38] S. J. Gulden, C. Riedele, S. Rollié, M.-H. Kopf, and H. Nirschl, "Online bubble size analysis in micro flotation," *Chem. Eng. Sci.*, vol. 185, pp. 168-181, 2018. https://doi.org/10.1016/j.ces.2018.04.009 ↑14, 15

[39] J. Ilonen *et al.*, "Comparison of bubble detectors and size distribution estimators," *Pat. Recognit. Lett.*, vol. 101, pp. 60-66, 2018. https://doi.org/10.1016/j.patrec.2017.11.014 ↑15

[40] X. Wang, C. Song, C. Yang, and Y. Xie, "Process working condition recognition based on the fusion of morphological and pixel set features of froth for froth flotation," *Miner. Eng.*, vol. 128, pp. 17-26, 2018. https://doi.org/10.1016/j.mineng.2018.08.017 ↑14, 15

[41] H. Zhang, Z. Tang, Y. Xie, X. Gao, and Q. Chen, "A watershed segmentation algorithm based on an optimal marker for bubble size measurement," *Measurement*, vol. 138, pp. 182-193, 2019. https://doi.org/10.1016/j.measurement.2019.02.005 ↑14, 15

[42] N. N. Misra, R. Phalak, and A. Martynenko, "A microscopic computer vision algorithm for autonomous bubble detection in aerated complex liquids," *J. Food Eng.*, vol. 238, pp. 54-60, 2018. https://doi.org/10.1016/j.jfoodeng.2018.06.007 ↑15

[43] L. Vinnett, J. Sovechles, C. O. Gomez, and K. E. Waters, "An image analysis approach to determine average bubble sizes using one-dimensional Fourier analysis," *Miner. Eng.*, vol. 126, pp. 160-166, 2018. https://doi.org/10.1016/j.mineng.2018.06.030 ↑14, 15

[44] M. de Langlard, H. Al-Saddik, S. Charton, J. Debayle, and F. Lamadie, "An efficiency improved recognition algorithm for highly overlapping ellipses: Application to dense bubbly flows," *Pat. Recognit. Lett.*, vol. 101, pp. 88-95, 2018. https://doi.org/10.1016/j.patrec.2017.11.024 ↑15

[45] N. Strokina, J. Matas, T. Eerola, L. Lensu, and H. Kälviäinen, "Detection of bubbles as concentric circular arrangements," *Machine Vision App.*, vol. 27, pp. 387-396, 2016. https://doi.org/10.1007/s00138-016-0749-7 ↑15

Jhonnatan Stiven Mera Campo

Received a degree in Physical Engineering from Universidad del Cauca in December 2021. He has a strong interest and orientation towards vision and artificial intelligence, in addition to instrumentation and control in industrial processes. He is currently working as an engineering analyst for one of the leaders in the field of vision and artificial intelligence, the Colombian company INTECOL SAS, located in the city of Medellín, developing artificial vision algorithms and industrial software for the quality inspection of products in different industries (among other use cases).

Email: jhonnatans@unicauca.edu.co

Jeimmy Adriana Muñoz Alegría

Received a degree in Physical Engineering in 2017 and a Master's degree in Industrial Automation in 2022, both from Universidad del Cauca. She is currently a PhD student in Energy, Water, and

Environment at Universidad de La Serena, Chile, with research interests in renewable energy, wastewater treatment technology, and the application of artificial intelligence in the environment.
Email: jeimymunoz@unicauca.edu.co

Juan Fernando Flórez Marulanda

Received a degree in Electronics and Telecommunications Engineering, specializing in Telematics Networks and Services and Industrial Computing, as well as a Master's degree in Electronics Engineering from Universidad del Cauca. He teaches at Universidad del Cauca since 1998, guiding subjects involving instrumentation, control, computer vision, and automation while advising degree works related to ISA, ISO, and IEEE standards and industrial process automation methodologies.
Email: jflorez@unicauca.edu.co

Elena Muñoz España

Received a degree in Electronics and Telecommunications Engineering and a Master's degree in Electronics Engineering from Universidad del Cauca. She is currently working as a full professor at Universidad del Cauca, Colombia. Her research interests include control systems, computer vision, and medical image processing.
Email: elenam@unicauca.edu.co